Theor Chem Acc (2007) 117:991–1000
DOI 10.1007/s00214-006-0213-2

REGULAR ARTICLE

Ab initio vibrational spectra and dielectric properties of carbonates: magnesite, calcite and dolomite

L. Valenzano · Y. Noël · R. Orlando · C. M. Zicovich-Wilson · M. Ferrero · R. Dovesi

Received: 6 July 2006 / Accepted: 13 October 2006 / Published online: 10 January 2007

Abstract The equilibrium geometry, the Raman and IR vibrational spectra at the Γ point, TO–LO splitting, IR intensities, Born and dielectric tensors of magnesite $MgCO_3$, dolomite $MgCa(CO_3)_2$ and calcite $CaCO_3$ have been calculated with the periodic ab initio program CRYSTAL, by using an all-electron gaussian type basis set and the B3LYP hamiltonian. LO (longitudinal-optical) modes are computed by correcting the dynamical matrix through Born charges and high frequency dielectric tensors obtained from well localized Wannier functions and a saw-tooth computational scheme. The mean absolute difference between calculated and experimental frequencies (IR TO and LO and RAMAN) is as small as 6.9 cm^{-1} for magnesite, 7.7 cm^{-1} for dolomite and 8.5 cm^{-1} for calcite. Calculated IR intensities are in semiquantitative agreement with experiment. The modes of the three compounds are compared through graphical animation available on the CRYSTAL website.

Keywords Vibrations · Carbonates · IR intensities · Dielectric tensor · Ab initio simulation

L. Valenzano
Dipartimento di Chimica IFM, Università di Torino and NIS (Nanostructured Interfaces and Surfaces), Via P. Giuria 5, 10125 Torino, Italy

Y. Noël
Laboratoire de Pétrologie, Modélisation de Matériaux et Processus, UMR 7160, Université Pierre et Marie Curie, 4 Place Jussieu, 75232 Paris cedex 05, France

R. Orlando
Dipartimento di Scienze e Tecnologie Avanzate, Università del Piemonte Orientale, Via Bellini 25/G, 15100 Alessandria, Italy

C. M. Zicovich-Wilson
Facultad de Ciencias, Universidad Autónoma del Estado de Morelos, Av. Universidad 1001, Col Chamilpa, 62210, Cuernavaca (MOR), Mexico

M. Ferrero
Dipartimento di Chimica IFM, Università di Torino and NIS (Nanostructured Interfaces and Surfaces), Via P. Giuria 5, 10125 Torino, Italy

R. Dovesi (✉)
Dipartimento di Chimica IFM, Università di Torino and NIS (Nanostructured Interfaces and Surfaces), Centre of Excellence, Via P. Giuria 7, 10125 Torino, Italy
e-mail: roberto.dovesi@unito.it
URL: http://www.nis.unito.it

1 Introduction

Magnesium and calcium carbonates are important sedimentary minerals. Calcite ($CaCO_3$) is one of the most common minerals, representing about 4% in weight of the Earth's crust and being part of many geological environments. Magnesite ($MgCO_3$) and calcite exhibit the same crystal structure and similar properties. Magnesite is usually abundant in rocks such as serpentine. Dolomite ($MgCa(CO_3)_2$) is a common sedimentary rock-forming mineral and massive layers of dolomite can be found in ancient rocks. For their large diffusion and simplicity, these minerals have been the subject of many experimental and theoretical investigations, with particular attention to thermodynamical properties [1–4] and vibrational spectra [2,5–9].

In the last few years, computational tools have been implemented in the CRYSTAL code [10] that permit to investigate vibrational spectra of crystalline compounds, and calcite [11,12] has been used, together with

$\alpha-$quartz [13,14], as a test system for calibrating the numerical parameters of the method and checking its accuracy. In the present paper, a previous study on calcite [12] is extended to magnesite and dolomite. Various features of the IR (LO and TO) and RAMAN spectra are compared along the family and thermodynamics of the reaction of $CaCO_3$ and $MgCO_3$ to give $MgCa(CO_3)_2$ is discussed. Animations are used to compare similar modes of the three compounds. All results have been obtained with CRYSTAL [10], an ab initio, periodic, all-electron package based on gaussian-type basis sets for representing crystalline orbitals. To the authors' knowledge, this is the first ab initio calculation of vibrational properties for this family of compounds.

The rhombohedral cell of magnesite (calcite) contains two $MgCO_3$ ($CaCO_3$) formula units and belongs to space group $R\bar{3}m$ (n.167). There are ten atoms in the unit cell and the 27 vibrational modes at Γ can be classified according to the irreducible representations of the $\bar{3}m$ point group as:

$$\Gamma_{\mathrm{tot}}^{\mathrm{MgCO_3}} = A_{1g} + 2A_{1u} + 3A_{2g} + 3A_{2u} + 4E_g + 5E_u$$

A_{1g} and E_g modes are Raman-active, A_{2u} and E_u are infrared-active, whereas A_{1u} and A_{2g} are spectroscopically inactive (silent modes).

Dolomite has a hexagonal cell containing one $MgCa(CO_3)_2$ unit (space group $R\bar{3}$, n.148) and its 27 vibrational modes can be classified according to the $\bar{3}$ point group as follows:

$$\Gamma_{\mathrm{tot}}^{\mathrm{MgCa(CO_3)_2}} = 4E_g + 4A_g + 5E_u + 5A_u$$

All modes are active either in Raman (A_g, E_g) or infrared (A_u, E_u).

This paper is organized as follows: Sect. 2 is devoted to the computational aspects; Sect. 3 is organized in subsections discussing equilibrium geometries, the relative stability of dolomite with respect to calcite and magnesite, Born and dielectric tensors, phonon frequencies at the Γ point, infrared intensities, the correlation of frequencies and intensities along the family of compounds.

2 Computational methods

Geometry optimization and spectra calculations were performed by means of the ab initio CRYSTAL code [10], which implements the Hartree-Fock and Kohn-Sham, Self Consistent Field (SCF) method for the study of periodic systems, and adopts a local basis set [15]. Calculations have been performed with the B3LYP hamiltonian [16,17]. The exchange-correlation contribution to the hamiltonian is evaluated by numerical integration, where radial and angular points of the integration grid are generated through Gauss-Legendre and Lebedev quadrature schemes, respectively. In this work, the same (75,974)p *pruned grid* was adopted as in previous studies of calcite [11,12], such a grid being labeled as XLGRID in the CRYSTAL manual [10]. The effect of the grid on the vibrational spectrum is discussed in Ref. [13], concerning α-quartz. The accuracy of such a grid can be estimated through the integrated charge density, that differs from the total number of electrons in the unit cell (84 for magnesite, 92 for dolomite and 100 for calcite) by 2×10^{-4} in all three cases.

All-electron basis sets have been used for all atoms: 8-6511(21), 6-311(11) and 8-411(11) contractions have been used for calcium, carbon and oxygen, respectively. These basis sets are reported in Ref. [12], where details about the gaussian function exponents are also provided. As regards magnesium, a 8-511(1) basis set has been used and the exponents of the most diffuse single gaussian shells are as follows: 0.688 (*sp*), 0.28 (*sp*) and 0.5 (*d*) [18].

Inner coordinates [19] and cell parameters (Table 1) have been optimized separately within an iterative procedure based on the total energy analytical gradients. The level of accuracy in evaluating the Coulomb and exchange series is controlled by five parameters [10], and the values used in the present calculations are 6, 6, 6, 6, 12. The reciprocal space has been sampled according to a regular sublattice with shrinking factor 6, corresponding to 40 independent **k** points in the irreducible Brillouin zone for dolomite, and 32 points for magnesite and calcite.

Calculation of the vibrational frequencies is performed within the harmonic approximation. For a detailed description of the method, we refer to previous papers [13,14]. Here, we simply remind that frequencies at the Γ point ($q = 0$) are obtained by diagonalizing the mass-weighted Hessian matrix W, whose $(\alpha i, \beta j)$ element is defined as:

$$W_{\alpha i,\beta j}(q=0) = \frac{H_{\alpha i,\beta j}}{\sqrt{M_\alpha M_\beta}} \tag{1}$$

where M_α and M_β denote the mass of atoms α and β, and i and j stand for x, y or z.

Total energy first derivatives with respect to the displacement coordinates $u_{\alpha j}$ of atoms from equilibrium geometry, $\upsilon_{\alpha j} = \partial V/\partial u_{\alpha j}$, are computed analytically, whereas second derivatives at $u_{\alpha j} = 0$ are calculated numerically as follows:

$$\left[\frac{\upsilon_{\alpha j}}{u_{\beta i}}\right]_0 \approx \frac{\upsilon_{\alpha j}(0,\ldots,u_{\beta i},\ldots)}{u_{\beta i}}$$

Table 1 Calcite, magnesite and dolomite equilibrium geometries

	Calcite	Exp [35]	Magnesite	Exp [30,31]	Dolomite	Exp [30,32]
a	5.0373	4.991(2)	4.6641	4.635(2)	4.8376	4.830(3)
c	17.3304	17.062(2)	15.2001	15.03(1)	16.2756	16.01(1)
V	380.8	368.1(3)	286.4	279.7(3)	329.9	323.2(4)
c/a	3.440	3.419(2)	3.259	3.243	3.364	3.315
z_C	–	–	–	–	0.24356	0.24289(7)
x_O	0.25565	0.2573(2)	0.27568	0.2778(2)	0.24537	0.2480(1)
y_O	–	–	–	–	−0.03780	−0.0354(1)
z_O	–	–	–	–	0.27754	0.24393(3)
d_{C-O}	1.2878	1.284(1)	1.2858	1.288(1)	1.2865	1.2858(5)
d_{Ca-O}	2.3907	2.3590(8)	–	–	2.4099	2.3816(5)
d_{Mg-O}	–	–	2.1241	2.1018(4)	2.1062	2.0821(5)

a and c are the lattice parameters (in Å), V is the volume of the crystallographic cell in Å^3, z_C is the fractional coordinate of the carbon atom in the primitive cell of dolomite, x_O, y_O and z_O are the fractional coordinates of the oxygen atoms, d_{i-j} indicate distances between atoms i and j (in Å). Experimental results are also reported for calcite [35], magnesite [30,31] and dolomite [30,32]

Since the energy variations corresponding to the displacements considered here (0.001 Å) can be as small as 10^{-6} to 10^{-7} hartree, the SCF cycle needs to be very well converged (10^{-10} hartree).

LO frequencies are obtained by adding a correcting non-analytical term ($W^{NA}_{\alpha i,\beta j}(q \to 0)$) to $W_{\alpha i,\beta j}(q = 0)$ (see Ref. [20] Sects. 5, 10, 34, 35; and Ref. [21]):

$$W^{NA}_{\alpha i,\beta j}(q \to 0) = \frac{1}{\sqrt{M_\alpha M_\beta}} \frac{4\pi}{\Omega} \frac{\left(\sum_k q_k Z^*_{\alpha,ki}\right)\left(\sum_{k'} q_{k'} Z^*_{\beta,k'j}\right)}{\sum_{kk'} q_k \varepsilon^\infty_{kk'} q_{k'}}$$

where

$$Z^*_{\alpha,ij} = \frac{\partial^2 V}{\partial E_i \partial u_{\alpha j}}$$

and E_i is a component of an applied external electric field. In the present case, q vectors are fully defined by symmetry, and coincide with the z and (x, y) directions.

As shown in the formula above, the additional term essentially depends on

(i) The electronic (clamped nuclei) dielectric tensor ϵ^∞, which was evaluated by using a finite field sawtooth model [22] with supercells of increasing size that have been used to check the convergence of the tensor components.
(ii) The *Born effective charge tensor* $Z^*_{\alpha,ij}$ obtained from well localized Wannier functions [23–26].

The intensity of the m-th IR-active mode is proportional to the square of the first derivative of the dipole moment μ with respect to the normal mode coordinate Q_m times the degeneracy d_m of the m-th mode:

$$A_m \propto d_m \left|\frac{\partial \mu}{\partial Q_m}\right|^2$$

Dipole moment derivatives are evaluated numerically by using unit cell localized Wannier functions [24,26].

The static dielectric tensor ϵ^0 is then obtained by adding to the high frequency term ϵ^∞ the ionic contribution, that depends on the eigenvalues (ω_m) and eigenvectors ($u_{\alpha i,m}$) of W, and on the atomic Born tensors ($Z^*_{\alpha,ij}$):

$$\varepsilon^0_{ij}(\omega) = \varepsilon^\infty_{ij} + \frac{4\pi}{\Omega_0} \sum_m \frac{\bar{Z}_{m,i}\bar{Z}_{m,j}}{\omega^2_m - \omega^2}$$

where

$$\bar{Z}_{m,j} = \sum_{\alpha i} \tilde{u}_{m,\alpha i} Z^*_{\alpha,ij}$$

and ω is the electric field frequency [note that m and (α, i) span the same set of $3N$ values, where N is the number of atoms in the cell].

Calculated TO and LO frequencies ν_v have been compared with experimental sets of M frequencies ν^{ref}_v through four global statistical indices defined as follows:

$$\bar{\Delta} = M^{-1} \sum_{v=1}^{M} \nu_v - \nu^{\text{ref}}_v$$

$$\overline{|\Delta|} = M^{-1} \sum_{v=1}^{M} \left|\nu_v - \nu^{\text{ref}}_v\right|$$

$$\begin{aligned} \Delta_{\max} &= \max\left(\nu_v - \nu^{\text{ref}}_v\right) \\ \Delta_{\min} &= \min\left(\nu_v - \nu^{\text{ref}}_v\right) \end{aligned} \qquad v = 1, 2, \ldots, M$$

where, $\bar{\Delta}$, $\overline{|\Delta|}$, $\Delta_{\max}$ and $\Delta_{\min}$ (all in cm^{-1}) are the mean difference, the mean absolute difference, and the maximum and minimum difference between the set of ν_v and ν^{ref}_v.

Visualization of structures has been dealt with the MOLDRAW program [27,28] and vibrational mode ani-

Table 2 Electronic (E_e) and zero point (ZPE) energies, and thermal contribution to the vibrational enthalpy (ΔH_0^{298}) (in Hartree per unit cell) for calcite, magnesite and dolomite. In the bottom rows, Δ refers to the formation of dolomite from calcite and magnesite

Crystal	E_e	ZPE	ΔH_0^{298}	Total
$2CaCO_3$	−1,883.092 441 663	0.035 965 505	0.008 630 458	−1,883.047 845
$2MgCO_3$	−928.108 132 780	0.039 022 188	0.007 009 432	−928.062 101
$CaMg(CO_3)_2$	−1,405.602 228 286	0.037 409 574	0.007 876 308	−1,405.556 942
$2CaCO_3 + 2MgCO_3$	−2,811.200 574 443	0.074 987 693	0.015 639 890	−2,811.109 946
$2CaMg(CO_3)_2$	−2,811.204 456 572	0.074 819 148	0.015 752 616	−2,811.113 884
$\Delta(E_h)$	−0.003 882	−0.000 168	0.000 113	−0.003 937
Δ(kJ/mol)	−10.192 191	−0.442 515	0.295 962	−10.336 593

The calculated formation enthalpy of dolomite is in excellent agreement with the experimental value [4] of -10.47 ± 1.20 kJ/mol

mations have been obtained by using the molecular viewer Jmol [29].

3 Results and discussion

3.1 Equilibrium geometry and relative stability

Calculated equilibrium geometries for calcite, magnesite and dolomite are reported in Table 1. The agreement with experiment [30–32] is excellent. The calculated *a* parameters, which are related to the strongly covalent CO_3 bonds, are larger than the experimental ones by 0.5% (magnesite), 0.2% (dolomite) and 1% (calcite) and the *c* lattice vector along the direction of the cation–anion–cation sequence is overestimated by about 1% (magnesite) and 1.5% (dolomite and calcite). As regards nearest neighbour distances, the maximum difference from experiment is 0.003, 0.03 and 0.02 Å for C–O, Ca–O and Mg–O, respectively.

In Table 2, the calculated data for estimating the formation enthalpy of dolomite from calcite and magnesite

$$2CaCO_3 + 2MgCO_3 \rightarrow 2CaMg(CO_3)_2 \qquad (2)$$

are reported: the total static energy as resulting from the SCF calculations, the zero point energy and the thermal vibrational contribution, as calculated from the vibrational eigenvalues according to standard thermodynamical formulas. Bottom rows in the table provide the formation enthalpy at 298 K (see Eq. (2)), where the zero point energy and thermal contribution for reactants and products are very similar, so that the formation enthalpy is dominated by the SCF static contribution. The present calculated result is in extremely good agreement with the accurate experimental datum measured by Navrotsky et al. [4] (−10.34 vs. -10.47 ± 1.20 kJ/mol).

3.2 Born and dielectric tensors, and Mulliken charges

The almost fully ionic nature of the three compounds is confirmed by Mulliken net charges of the cations (about +1.7|*e*|). The compensating −1.7|*e*| net charge of the strongly covalent CO_3 group results from +0.7|*e*| for carbon and −0.8|*e*| for oxygen. Bond population is +0.74 |*e*| for C–O and +0.07|*e*| (+0.02|*e*|) for Mg–O (Ca–O).

Table 3 Atomic Born effective charge tensors for magnesite

Mg	C	O
$\begin{pmatrix} 2.30 & 0.28 & 0.00 \\ -0.28 & 2.30 & 0.00 \\ 0.00 & 0.00 & 2.11 \end{pmatrix}$	$\begin{pmatrix} 3.10 & 0.00 & 0.00 \\ 0.00 & 3.10 & 0.00 \\ 0.00 & 0.00 & 0.58 \end{pmatrix}$	$\begin{pmatrix} -2.08 & 0.51 & -0.08 \\ 0.51 & -1.49 & -0.14 \\ -0.05 & -0.10 & -0.90 \end{pmatrix}$

The average value of the diagonal elements are +2.24|*e*| (Mg), +2.26|*e*| (C), −1.49|*e*| (O)

Calculated Born effective charge atomic tensors for magnesite only are reported in Table 3, the other two compounds showing similar Born charges. The Mg (Ca) tensor is nearly diagonal, and isotropic, with the mean value of the diagonal elements being +2.24|*e*|, *i.e.* slightly larger than the formal charge (+2|*e*|). The C tensor is diagonal by symmetry and strongly anisotropic (the largest difference among diagonal elements is 2.8|*e*|). Also oxygen is strongly anisotropic, with large off-diagonal elements.

High frequency and static dielectric tensors at $T = 0$ K of the three compounds have been calculated with a 60 atom supercell for the ϵ_{xx}^{∞} and ϵ_{yy}^{∞} components and with a 30 atom supercell for ϵ_{zz}^{∞}. The results reported in Table 4 are stable within 0.001 with respect to the use of larger supercells. Overall, high frequency and static dielectric tensor components are between 3 and 20% smaller than the experimental values [5,33] measured at room temperature.

3.3 Vibrational spectrum of magnesite, dolomite, calcite: classification and comparison with experiment

The calculated and experimental spectra of the three compounds are reported in Tables 5 and 6, whereas IR

Table 4 Calculated and experimental high frequency and static dielectric tensors of calcite, magnesite and dolomite

		ϵ^{∞}				ϵ^{0}			
Crystal	Comp.	This work	Exp.[a]	Exp.[b]	Δ%	This work	Exp.[c]	Exp.[b]	Δ%
Calcite	*xx*	2.6	2.7	2.7	4	7.8	8.5	9.0	8
	zz	2.1	2.2	2.4	4	6.4	8.0	9.0	20
Magnesite	*xx*	2.7	2.9	2.8	7	7.2	–	8.3	13
	zz	2.1	2.3	2.5	9	6.0	–	6.5	8
Dolomite	*xx*	2.6	2.8	2.8	7	6.5	8.0	8.0	19
	zz	2.1	2.2	2.5	4	6.6	6.8	7.1	3

Δ% is the percentage difference of the calculated data with respect to the most recently available experimental results [33,36]

[a] Ref. [36]

[b] Ref. [5]

[c] Ref. [33]

intensities are given in Table 7. So far the CRYSTAL code does not provide RAMAN intensities.

The carbonate spectrum can be divided into two frequency regions, separated by about 400 cm^{-1}. Frequencies lower than 311 (calcite), 354 (dolomite) and 365 cm^{-1} (magnesite) correspond to "external" modes, and result from the combination of Ca/Mg and CO_3 translations (T) with CO_3 rotations (R), whereas frequencies larger than 711 (calcite), 722 (dolomite) and 736 cm^{-1} (magnesite) correspond to "internal" modes (I) of CO_3.

Under the hypothesis of full mode separability, the 12 internal modes, 6 CO_3 rotations and the 9 Ca/Mg and CO_3 translations for calcite and magnesite can be classified as follows:

$$\begin{aligned} 9\ \text{translations}\ (T): &\quad A_{2g}+A_{1u}+A_{2u}+E_g+2E_u \\ 6\ \text{rotations}\ (R): &\quad A_{2g}+A_{2u}+E_g+E_u \\ 12\ \text{internal}\ (I): &\quad A_{1g}+A_{2g}+A_{1u}+A_{2u}+2E_g+2E_u \end{aligned}$$

For dolomite the classification becomes

$$\begin{aligned} 9\ \text{translations}\ (T): &\quad A_g+2A_u+E_g+2E_u \\ 6\ \text{rotations}\ (R): &\quad A_g+A_u+E_g+E_u \\ 12\ \text{internal}\ (I): &\quad 2A_g+2A_u+2E_g+2E_u \end{aligned}$$

However, T modes couple to R modes with the same symmetry at some extent (see below and Ref. [12]), because they span the same energy range.

A complete classification of calcite modes has been provided in Ref. [11,12], and animation of the modes is available at the CRYSTAL web-site [34].

A similar classification applies also to magnesite and dolomite. However, modes appear in different sequential order and frequencies shift progressively along the series calcite-dolomite-magnesite, as we will discuss in the next subsection.

The bottom part of Tables 5 and 6 contains the statistics about a comparison of the present calculated data with the excellent experimental results by Hellwege et al. [5]. The mean absolute difference $\overline{|\Delta|}$ is smaller than 9 cm^{-1} in all cases. The worst agreement between calculated and experimental frequency values of the full set is observed for the four lowest frequency modes of calcite (two TO, two LO, with E_u and A_{2u} symmetry), with differences between 17 and 34 cm^{-1}. For magnesite, the largest error (Table 5) is 16 cm^{-1}, and it is 18.5 cm^{-1} for dolomite (Table 6). As discussed in Ref. [12], temperature effects are not responsible for this large discrepancy and its origin remains unclear. Results for the corresponding modes of magnesite and dolomite show smaller overestimations with respect to the experimental values (Tables 5 and 6): 7–16 and 10–15 cm^{-1}, respectively. The frequency of the lowest E_u and A_{2u} modes of magnesite and dolomite are, however, 50–120 cm^{-1} higher than for calcite. This suggests either possible problems in the experimental determinations at very low wavenumbers or an important role of dispersion forces, not taken into account in our model, that would nevertheless become negligible for modes just above 150–200 cm^{-1}, where the agreement with experiment improves dramatically. So far no evidence supporting either of the two hypotheses is available.

Calculated and experimental IR intensities for the three carbonates are listed in Table 7. The calculated data have been rescaled by a common factor f so defined

$$f = \frac{1}{N}\sum_{i=1}^{N}\frac{f_i^{\text{calc}}}{f_i^{\text{exp}}}$$

with $N = 8$ for calcite and magnesite and $N = 9$ for dolomite. A semiquantitative agreement is observed in the three cases, that is to be considered very satisfactory,

Table 5 Raman (R), infrared (I) and silent (S) frequencies for calcite and magnesite

		Calcite			Magnesite		
		ν	$\Delta\nu$	Exp	ν	$\Delta\nu$	Exp
	E_g	155.9	−0.1	156	207.4	−4.6	212
	E_g	276.6	−7.4	284	324.9	−7.1	332
R	E_g	710.9	−1.1	712	736.0	1.0	735
	A_{1g}	1,088.4	2.4	1,086	1,100.3	4.3	1,096
	E_g	1,432.4	−1.6	1,434	1,446.9	−13.1	1,460
	E_u	124.9	22.9	102	240.9	15.9	225
		139.6	16.6	123	249.5	8.5	241
	A_{2u}	126.1	34.1	92	240.6	10.6	230
		159.5	23.5	136	287.6	6.6	281
	E_u	219.6	−3.4	223	298.7	−2.3	301
		230.7	−8.3	239	301.3	−13.7	315
I	E_u	285.9	−11.1	297	343.1	−12.9	356
		379.4	−1.6	381	473.7	−1.3	475
	A_{2u}	298.9	−4.1	303	348.4	−13.6	362
		402.6	15.6	387	457.8	−1.2	459
	E_u	711.5	−0.5	712	744.1	−2.9	747
		712.9	−2.1	715	747.3	−15.7	763
	A_{2u}	874.4	2.4	872	874.8	−1.2	876
		894.2	4.2	890	910.4	−0.6	911
	E_u	1,400.1	−6.9	1,407	1,429.1	−6.9	1,436
		1,554.4	9.4	1,549	1,600.7	1.7	1,599
	A_{2g}	192.9			311.3		
	A_{1u}	288.6			364.8		
S	A_{2g}	311.4			359.3		
	A_{2g}	882.3			888.2		
	A_{1u}	1,088.3			1,099.7		
	$\overline{\lvert\Delta\rvert}$		8.5			6.9	
	$\bar{\Delta}$		3.9			−2.3	
	$\Delta_{\min}$		−11.1			−15.7	
	$\Delta_{\max}$		34.1			15.9	

$\Delta\nu$ is the difference (in cm^{-1}) with respect to the available experimental data [5]

as intensities span a range as large as two orders of magnitude.

3.4 Vibrational spectrum of magnesite, dolomite, calcite: trends along the series

Figures 1, 2 and 3 show how corresponding peaks shift to higher wavenumbers in going from calcite to magnesite through dolomite. The three carbonates show a similar pattern in the upper part of the TO-IR and RAMAN spectra, with a shift to higher frequencies ranging from 10 to 30 cm^{-1} (Tables 5 and 6) for the three bands above 700 cm^{-1}. The LO shift is larger. It can be as large as 50 cm^{-1}, because the electrostatic effects are stronger in magnesite, as a consequence of its smaller unit cell volume. Larger differences are observed in the lower part of the spectrum. For example, the lowest calculated wavenumber is 125 cm^{-1} for calcite and 241 cm^{-1} for magnesite. Figure 1 shows that bands shift by different amounts. Therefore, labels have been added to facilitate the identification of corresponding peaks in the three systems ("bis" labels peaks appearing in the spectrum of dolomite because of its lower symmetry). Trends in the IR intensities are very regular along the family: they increase from calcite to magnesite for peak 1 and 2, whereas they decrease for peak 3 and 4 and increase again for peak 5. A similar regular trend is shown by LO intensities, although here the calcite < dolomite < magnesite order (or viceversa) is not observed in general. So far, no discussion of intensities in the Raman spectrum can be done as RAMAN intensities are not yet available from the CRYSTAL code. The peaks of the three compounds in Fig. 3 have been represented with different intensity arbitrarily, just for clarity of representation.

By analyzing the possible origin of the frequency differences among the three systems, we can suppose schematically that there is

Table 6 RAMAN (R) and infrared (I) frequencies for dolomite

		Dolomite		
		ν	$\Delta\nu$	Exp [5]
	E_g	177.0	1.0	176
	A_g	235.2	–	–
	E_g	295.5	−5.5	301
	A_g	335.8	0.8	335
R	E_g	722.5	−1.5	724
	A_g	888.2	8.2	880 [2]
	A_g	1,101.0	2.0	1,099
	E_g	1,437.7	−6.3	1,444
	A_u	158.6	12.6	146
		204.7	11.7	193
	E_u	165.3	15.3	150
		186.9	13.9	173
	E_u	256.1	1.1	255
		264.5	−6.5	271
	A_u	302.7	−11.3	314
		321.4	−3.6	325
	E_u	339.4	−4.8	345
		449.6	10.6	439
I	A_u	353.8	−7.2	361
		439.5	10.5	429
	E_u	726.6	−1.4	728
		729.1	−11.9	741
	A_u	877.6	−1.4	879
		904.8	3.8	901
	A_u	1,096.7	−3.3	1,100 [7]
		1,096.7	–	–
	E_u	1,416.5	−18.5	1,435
		1,581.5	1.5	1,580
	$\overline{\lvert\Delta\rvert}$		6.8	
	$\bar{\Delta}$		0.4	
	$\Delta_{\min}$		−18.5	
	$\Delta_{\max}$		15.3	

$\Delta\nu$ is the difference (in cm^{-1}) with respect to experimental data [2,5,7]. Experimental data corresponding to the calculated Raman A_g mode at 235.2 cm^{-1} (273 cm^{-1} from Ref. [6], giving $\Delta\nu = -37.8\,cm^{-1}$) is not reported in the table and it has been excluded from statistics

- a unit cell volume effect (the ionic radius of Mg is much smaller than that of Ca and, as a consequence magnesite unit cell volume is smaller than dolomite and calcite volumes), such that the smaller the volume, the stronger the electrostatics, which implies steeper potential wall and higher frequencies
- a mass effect, as mass appears in the denominator of the dynamical matrix (Eq. (1))
- a chemical effect, as Ca and Mg have different electronegativity.

Data in Table 8 are helpful in such analysis. In an attempt to separate and estimate mass effects, we have re-calculated the vibrational spectrum of calcite by assigning the mass of magnesium to Ca ions in Eq. (1) and, viceversa, the spectrum of magnesite by assigning the mass of Ca to Mg ions.

For symmetry reasons, Ca and Mg cations do not participate in gerade modes (see animations at the CRYSTAL web-site) [34] and the wavenumbers corresponding to these modes are invariant to a change of cation mass (compare columns 1–2, and 4–5 in Table 8). Differences between calcite (column 1) and magnesite (column 5) are then due to unit cell volume or "chemical" effects. However, since all three carbonates have similar Born and Mulliken charges, we can suppose that "chemical" effects are much less important. For the "internal" modes (stretching and bending in CO_3), this shift between the two spectra is small: 25, 6, 12 and 14 cm^{-1} for calcite modes at 710, 882, 1,088 and 1,432 cm^{-1}, respectively. For the "external" gerade modes the volume effect is larger, i.e. of the order of 50 cm^{-1} for the modes at 155, 276 and 311 cm^{-1} and it extends to 120 cm^{-1} for the A_g mode at 192 cm^{-1}, this last mode corresponding to a vertical translation-rotation of the CO_3 group (see animation at Ref. [34]). For the ungerade "internal" CO_3 modes, to which Ca and Mg cations give essentially no contribution, the shift from column 1–5 is similar to that for the gerade modes: 33, 0, 10, 28 cm^{-1} for modes at 711, 874, 1,088, 1400 cm^{-1} of calcite.

The only subset for which both mass and volume effects are active are ungerade "external" modes. Mass effect is limited for the A_u mode at 126 cm^{-1} and the E_u mode at 124.9 cm^{-1} (minor participation of the cation to these modes, i.e. mostly translations-rotations of the CO_3 group, with a syncronous cation movement with the center of mass at rest). However, the volume effect is larger than for all other modes discussed so far (120 and 100 cm^{-1}, respectively).

For the six modes with the largest cation participation ("translation modes" of cations) the mass effect is similar or larger than the volume effect: the E_u mode at 219 cm^{-1} of calcite increases by 80 cm^{-1} in magnesite, but 60 of 80 cm^{-1} are due to mass effects (277.9 cm^{-1} in column 2). Similarly, the A_u mode at 299 cm^{-1} increases to 348 cm^{-1} in magnesite (38 out of 50 cm^{-1} due to mass effects) and a similar behavior is shown by the E_u mode at 285 cm^{-1} of calcite (shift of 50 cm^{-1}, mass effect of 40 cm^{-1}). Finally the A_u (A_{1u} in the full calcite symmetry) mode at 288 cm^{-1} shifts to 364, the largest part of the shift being due to a mass effect.

In summary, the shift of individual modes is in no case larger than 120 cm^{-1}. However, it varies for the different modes, so that the sequential order of peaks can be altered and the low frequency part of the spectra of the three compounds may appear as quite different, as shown by Figs. 1, 2 and 3.

Table 7 IR intensities for calcite, magnesite and dolomite

		Calcite			Dolomite			Magnesite		
		Calc.	Exp.	Δ	Calc.	Exp.	Δ	Calc.	Exp.	Δ
	2	2.9	3.1	−0.2	5.5	4.9	0.6	5.4	6.2	−0.8
	5	4.1	5.1	−1.0	3.0	4.6	−1.6	3.1	6.7	−3.6
E_u	9	16.2	14.6	1.6	23.3	20.3	3.0	40.5	26.4	14.1
	12	0.6	0.52	0.08	1.0	1.9	−0.9	1.7	3.1	−1.4
	17	106.6	108.9	−2.3	120.0	115.5	5.1	169.2	125.6	43.6
	1	4.2	4.2	0.0	5.9	3.2	2.7	17.4	13.9	3.5
$A_{(2)u}$	7	14.1	12.8	1.3	7.3	6.8	0.5	15.5	14.5	1.0
	13	6.5	6.7	−0.2	8.7	9.4	−0.7	14.9	13.1	1.8
	10	–	–	–	8.3	10.0	−1.7	–	–	–
$\overline{\lvert\Delta\rvert}$				0.8			1.9			8.7

Modes are labeled as in Table 8. $\overline{\lvert\Delta\rvert}$ is the mean absolute difference between calculated and experimental [5] data

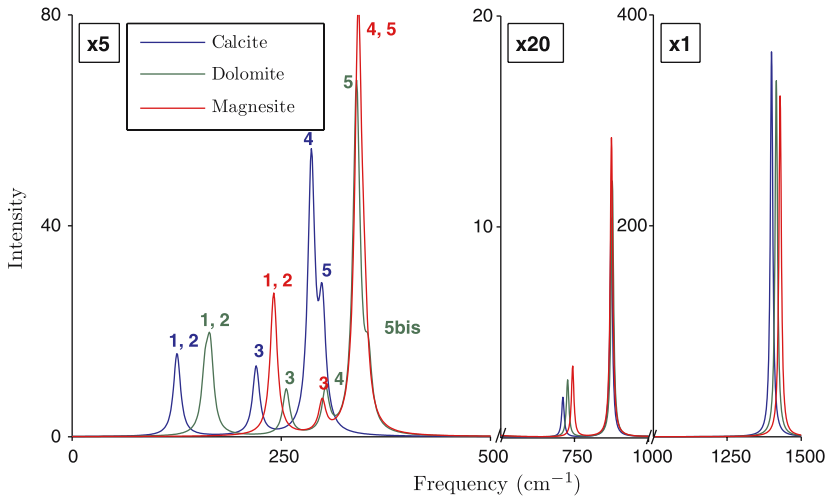

Fig. 1 Calculated infrared TO spectrum of magnesite, dolomite and calcite. Intensities have been magnified by a factor 5 in the 0–500 cm^{-1} region of the spectrum, and by a factor 20 in the 500–1,000 cm^{-1} interval. For clarity peaks have been labeled in a sequential order and dolomite extra peaks (symmetry is lower than for calcite and dolomite) are indicated as "bis"

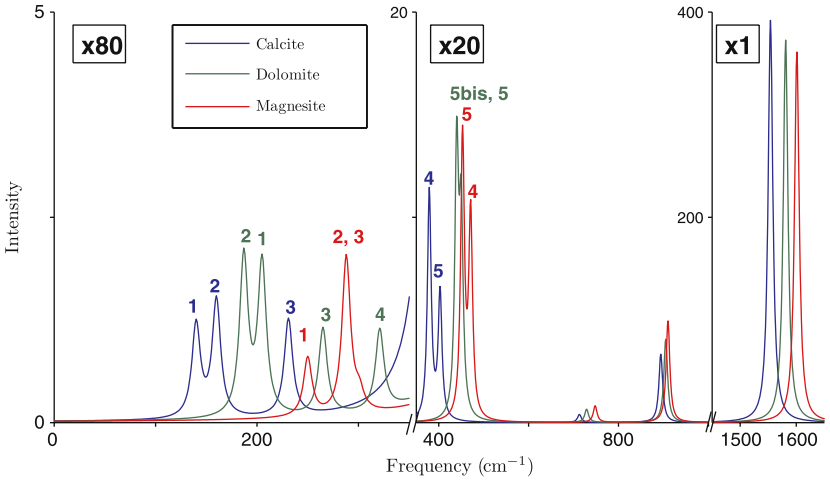

Fig. 2 Calculated infrared LO spectrum of magnesite, dolomite and calcite. Intensities have been magnified by a factor 80 in the 0–350 cm^{-1} region of the spectrum, and by a factor 20 in the 350–1,000 cm^{-1} interval. For clarity peaks have been labeled in a sequential order and dolomite extra peaks (symmetry is lower than for calcite and dolomite) are indicated as "bis"

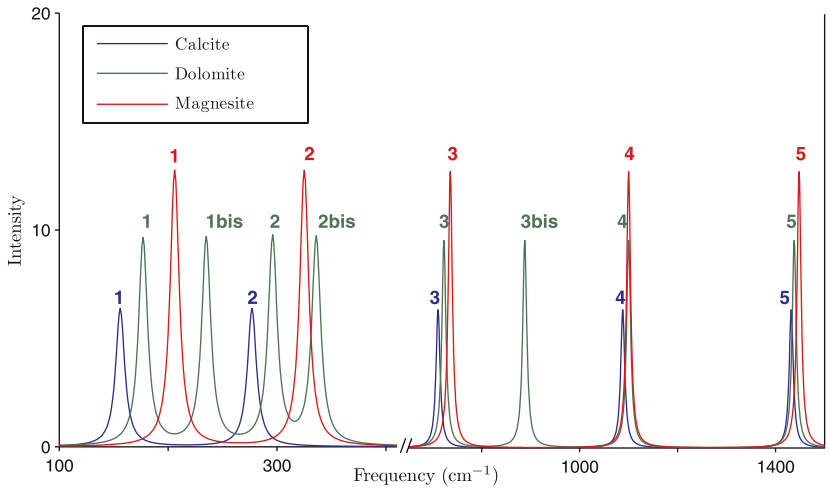

Fig. 3 Calculated Raman spectrum for magnesite, dolomite and calcite. Intensities are assigned arbitrarily. See Figs. 1 and 2 for peak labels

Table 8 TO modes of calcite, dolomite and magnesite as such, and when a cation mass is substituted in the mass weighted hessian matrix before diagonalization

Modes		Calcite		Dolomite	Magnesite	
		Ca_2	Mg_2	MgCa	Ca_2	Mg_2
1	A_u	126.1	132.6	158.6	215.3	240.6
2	E_u	124.9	132.6	165.3	224.6	240.9
3	E_g	155.9	155.9	177.0	207.4	207.4
4	A_g	192.9	192.9	235.2	311.2	311.3
5	E_u	219.5	277.9	256.1	237.0	298.7
6	E_g	276.6	276.6	295.5	324.9	324.9
7	A_u	298.9	336.2	302.7	282.6	348.4
8	A_g	311.4	311.4	335.8	359.3	359.3
9	E_u	285.9	324.5	339.4	305.7	343.1
10	A_u	288.5	372.2	353.8	330.9	364.8
11	E_g	710.9	710.9	722.5	736.0	736.0
12	E_u	711.5	711.8	726.6	744.1	744.1
13	A_u	874.4	874.4	877.6	874.7	874.8
14	A_g	882.3	882.3	888.2	888.2	888.2
15	A_u	1,088.3	1,089.0	1,096.7	1,098.6	1,099.7
16	A_g	1,088.4	1,088.4	1,101.0	1,100.3	1,100.3
17	E_u	1,400.1	1,400.4	1,416.5	1,428.8	1,429.1
18	E_g	1,432.4	1,432.4	1,437.7	1,446.9	1,446.9

In column two (Mg), for example, the magnesium mass has been used in the denominator of the calcite weighted hessian matrix. The effect of the pure mass substitution is then evidentiated. Frequencies for the three systems are labeled according to the space group of dolomite ($R\bar{3}$)

4 Conclusions

The vibrational spectrum of magnesite, dolomite and calcite, and many related properties, have been investigated with an all electron, local basis set and the B3LYP hamiltonian by using the CRYSTAL code.

RAMAN and infrared (LO–TO) spectra of the three compounds, IR intensities and dielectric tensors are in excellent agreement with experiment. Trends along the family have been discussed and interpreted. The various modes can be analyzed by means of tools recently implemented in the CRYSTAL code, including isotopic substitution and graphical animation, that provide a full characterization of the spectrum. The present study shows that the compelte characterization of the dynamics of large unit cell crystalline systems is now within reach.

Acknowledgements R. Dovesi and L. Valenzano acknowledge Italian MURST for financial support (Cofin04 Project 25982_002 coordinated by Prof. R. Resta). LV also thanks Dr. B. Civalleri for helpful discussions. Computer support from the CINECA (RD and LV) and CINES (Y. Noel) supercomputing centers is kindly acknowledged.

References

1. Zhang J, Martinez I, Guyot F, Gillet P, Saxena SK (1997) Phys Chem Min 24:122–130
2. Matas J, Gillet P, Ricard Y, Martinez I (2000) Eur J Mineral 12:703–720
3. Gillet P, McMillan P, Schott J, Badro J, Grzechnik A (1996) Geochim Cosmochim Acta 60:3471–3485
4. Chai L, Navrotsky A, Reeder RJ (1995) Geochim Cosmochim Acta 59:939–944
5. Hellwege KH, Lesch W, Plihal M, Schaack G (1970) Z Physik 232:61–86
6. Nicola JH, Scott JF, Couto RM, Correa MM (1976) Phys Rev B 14:4676–4678
7. Bottcher ME, Gehlken P-L, Steele DF (1997) Solid State Ionics 101:1379–1385
8. Pilati T, Demartin F, Gramaccioli CM (1998) Acta Crystallogr Sec B 54:515–523
9. Pavese A, Catti M, Price GD, Jackson RA (1992) Phys Chem Min 19:80–87
10. Dovesi R, Saunders VR, Roetti C, Orlando R, Zicovich-Wilson CM, Pascale F, Civalleri B, Doll K, Harrison NM, Bush IJ, D'Arco P, Llunell M (2006) Crystal06 user's manual. Università di Torino, Torino
11. Prencipe M, Pascale F, Zicovich-Wilson C, Saunders VR, Orlando R, Dovesi R (2004) Phys Chem Min 31:559–564
12. Valenzano L, Torres JA, Doll K, Pascale F, Zicovich-Wilson CM, Dovesi R (2006) Zeitschrift Phisikalische Chemie 220:893–912
13. Pascale F, Zicovich-Wilson CM, Gejo FL, Civalleri B, Orlando R, Dovesi R (2004) J Comp Chem 25:888–897
14. Zicovich-Wilson CM, Pascale F, Roetti C, Saunders VR, Orlando R, Dovesi R (2004) J Comp Chem 25:1873–1881
15. Pisani C, Dovesi R, Roetti C (1988) Hartree-Fock ab-initio treatment of crystalline systems, vol 48. Lecture notes in chemistry. Berlin Heildelberg New York, Springer
16. Becke AD (1993) J Chem Phys 98:5648–5652
17. Becke AD (1988) J Chem Phys 88:2547–2553
18. Prencipe M private communication
19. Civalleri B, D'Arco P, Orlando R, Saunders VR, Dovesi R (2001) Chem Phys Lett 348:131–138
20. Born M, Huang K (1954) Dynamical theory of crystal lattices. Oxford University Press, Oxford
21. Umari P, Pasquanello A, Corso AD (2001) Phys Rev B 63:094305
22. Darrigan C, Rérat M, Mallia G, Dovesi R (2003) J Comp Chem 24:1305–1312
23. Baranek P, Zicovich-Wilson C, Roetti C, Orlando R, Dovesi R (2001) Phys Rev B 64:125102
24. Zicovich-Wilson CM, Dovesi R, Saunders VR (2001) J Chem Phys 115:9708–9719
25. Nöel Y, Zicovich-Wilson C, Civalleri B, D'Arco P, Dovesi R (2002) Phys Rev B 65:014111
26. Zicovich-Wilson CM, Bert A, Roetti C, Dovesi R, Saunders VR (2002) J Chem Phys 116:1120–1127
27. Moldraw program. http://www.moldraw.unito.it/
28. Ugliengo P, Viterbo D, Chiari G (1993) Z Kristallogr 207:9–23
29. Jmol program. http://www.jmol.org/
30. Fiquet G, Guyot F, Itie J-P (1994) Am Mineral 79:15–23
31. Markgraf SA, Reeder RJ (1985) Am. Mineral 70:590–600
32. Reeder RJ, Markgraf SA (1986) Am. Mineral 71:795–804
33. Lide DR (1991-1992) CRC handbook of chemistry and physics. CRC Press Inc., USA
34. Calcite, dolomite, magnesite animations. http://www.crystal.unito.it/vibs/carbonates
35. Maslem EN, Streltsov VA, Streltsova NR (1993) Acta Crystallogr Sec B 49:636–641
36. Deer WA, Howie RA, Zussman J (1992) An introduction to the rock-forming minerals. Longman Group, England